Ab initio modeling of quantum transport properties of molecular electronic devices

Jeremy Taylor,[1] Hong Guo,[1] and Jian Wang[2]
[1]*Center for the Physics of Materials and Department of Physics, McGill University, Montreal, PQ, Canada H3A 2T8*
[2]*Department of Physics, The University of Hong Kong, Pokfulam Road, Hong Kong, China*
(Received 25 October 2000; revised manuscript received 8 January 2001; published 1 June 2001)

We report on a self-consistent *ab initio* technique for modeling quantum transport properties of atomic and molecular scale nanoelectronic devices under external bias potentials. The technique is based on density functional theory using norm conserving nonlocal pseudopotentials to define the atomic core and nonequilibrium Green's functions (NEGF's) to calculate the charge distribution. The modeling of an *open* device system is reduced to a calculation defined on a finite region of space using a screening approximation. The interaction between the device scattering region and the electrodes is accounted for by self-energies within the NEGF formalism. Our technique overcomes several difficulties of doing first principles modeling of open molecular quantum coherent conductors. We apply this technique to investigate single wall carbon nanotubes in contact with an Al metallic electrode. We have studied the current-voltage characteristics of the nanotube-metal interface from first principles. Our results suggest that there are two transmission eigenvectors contributing to the ballistic conductance of the interface, with a total conductance $G \approx G_0$ where $G_0 = 2e^2/h$ is the conductance quanta. This is about half of the expected value for infinite perfect metallic nanotubes.

DOI: 10.1103/PhysRevB.63.245407 PACS number(s): 72.10.−d, 85.65.+h

I. INTRODUCTION

In the last several years, there has been a large growth of research effort in nanotechnology, and in particular, the search for nanoelectronic devices has become a worldwide effort.[1] Such an effort is made viable by the ability to fabricate device structures of truly nanometer scale,[2,3] by the discoveries of self-organized nanostructures such as carbon nanotubes,[4] and by the progress in making accurate measurements of structural and electronic properties of these nanosystems. More recently, quantum transport measurements on atomic and molecular scale nanoelectronic systems have received great attention[5–12] because they represent the ultimate size limit of functional devices. The current-voltage (*I-V*) characteristics of these atomic and molecular systems have profound potential for device application, including high nonlinearity, negative differential resistance, electromechanic and electrostatic current switching.[5–8,11] Demonstrations of molecular based logic gates[5] and nonvolatile random access memory device[8,6] have already been made, and clearly point to the exciting possibility of molecular computing machinery.[5] Previous work also clearly demonstrated that many of the molecular device characteristics are directly related to specific atomic scale degrees of freedom, and interactions of the device region with the device electrodes play one of the most important roles. From the theoretical point of view, a serious challenge is to accurately predict quantum transport properties of atomic/molecular scale devices including the *I-V* curves, without any phenomenological parameters. This goal, despite extensive research,[13–35] has not yet been achieved satisfactorily.

In this paper, we present a modeling technique which solves the theoretical challenge within the first principles density functional theory (DFT) (Refs. 36–38) approach. To make the problem at hand clear, we use the molecular device shown in Fig. 1 to discuss our technique. Figure 1 represents a typical two-probe molecular device geometry where a semi-infinite armchair carbon nanotube is in contact with an atomic scale semi-infinite Al metallic electrode. The interface region (central box) can be considered as a ''molecule'' in contact to a metallic electrode on the left, and to a nanotube electrode on the right.[39] These electrodes extend to electron reservoirs at $z = \pm\infty$ where the electric current is collected. A gate electrode with potential V_g which is capacitively couple to the molecule, may also be present. For concreteness, we assume a two probe geometry in what follows and fix the transport direction to be along the z axis. Extensions to different boundary conditions are straightforward and will be presented elsewhere.[40] Our theoretical goal is to predict quantum transport properties of molecular nanodevices such as that of Fig. 1, including their *I-V* characteristics, from first principles without phenomenological parameters.

To analyze quantum transport through molecular scale de-

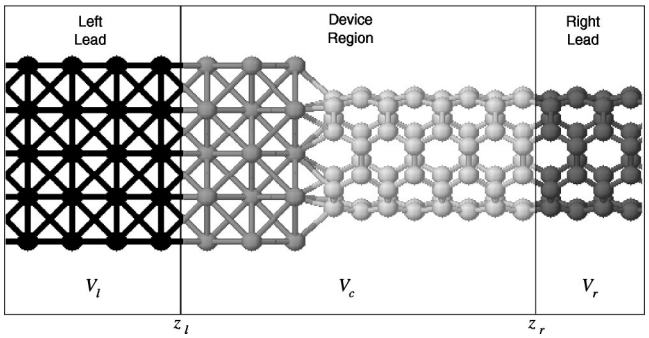

FIG. 1. Metallic electrode-nanotube interface. A semi-infinite (4,4) armchair nanotube is in contact with a semi-infinite Al(100) metallic electrode. This is a typical two probe molecular device structure where the device region (the center box) is coupled to perfect atomic-scale electrodes which extend to reservoirs at $z = \pm\infty$, where current is collected. Bias potentials, $\Delta V_{l/r}$ may be applied to the reservoirs. Furthermore, the device may be capacitively coupled to a gate electrode through a gate potential.

vices from first principles under a finite bias potential, three points are of essential importance. First, one must deal with *open* systems within the DFT formalism. Recall that conventional DFT methods (e.g., the well-known plane wave methods discussed in Ref. 41 or real-space techniques such as Ref. 42) can treat two kinds of problems: (i) finite systems such as an isolated molecule, as in quantum chemistry and (ii) periodic systems consisting of supercells, as in solid state physics. In contrast, a molecular device, such as that shown in Fig. 1, has *open* boundaries provided by long electrodes which maintain different chemical potential due to an external bias. In other words, a typical device geometry is neither isolated nor periodic. Therefore, one must find a technique beyond (i),(ii) above, to reduce the infinitely large problem of an open device to a finite problem which can be efficiently dealt with. Second, one must calculate the device Hamiltonian $H[\rho(\mathbf{r})]$ within DFT using the correct charge distribution $\rho(\mathbf{r})$ which must be constructed under a finite bias with the correct open boundary conditions. For open systems, $\rho(\mathbf{r})$ is contributed by both scattering states which connect $z=-\infty$ to $z=+\infty$ crossing the molecular region, and by bound states which may exist inside the molecular region. It is worth noting that when the electrochemical potentials $\mu_{l/r}+\Delta V_{l/r}$ of the two electrodes are not equal, the device is actually in a nonequilibrium state. Here $\Delta V_{l/r}$ is the bias voltage applied at the left/right reservoirs and $\mu_{l/r}$ is the chemical potentials there. In this work, we will not consider transient phenomena and only focus on the steady state. Third, an efficient numerical procedure should be used in order to simulate molecular devices with a large number of atoms.

Similar to the pioneering work of Lang,[30] the formalism developed in this work is based on a self-consistent solution of the Kohn-Sham (KS) equation for *open* systems. However, we do not use the jellium approximation to describe the electrodes but we assume that each semi-infinite electrode has its own discrete translational symmetry, represented by a collection of atoms at positions $\{\mathbf{R}_I\}$ in a unit cell repeated to either $z=+\infty$ or $z=-\infty$. The use of atomic scale electrodes complicates the problem considerably because of its nontrivial electronic structure and multiple van Hove singularities in the density of states of the electrodes. Previous methods[30,31] construct charge density from eigenstates of the open system where bound states contribution has been neglected.[30,31] In this work, we apply the nonequilibrium Green's functions (NEGF's) (Refs. 43–45) which naturally include scattering states as well as bound states contributions to the charge density.

We have applied our NEGF-DFT *ab initio* formalism to investigate quantum transport properties of a C_{60} based molecular junction in the ballistic regime, a short account of these results can be found in Ref. 39. In the following, we apply our formalism to investigate the transport properties of a single wall carbon nanotube (SWCN) in contact with a Al metallic electrode shown in Fig. 1. We report the *I-V* characteristics of the nanotube-metal interface from first principles. We found that there are two transmission eigenvectors[46,47] contributing to the ballistic conductance of the SWCN-metal interface, with a total conductance $G \approx G_0$ where $G_0=2e^2/h$ is the conductance quanta. This is about half of the expected value for *infinite* perfect metallic nanotubes. This result is consistent with a previous calculation using the supercell method[28] on a jellium-nanotube interface, and provides a possible explanation of the phenomenon observed by Frank *et al.*[48]

The rest of the paper is organized as follows. In Sec. II, we present a discussion of the theoretical formalism. Section III presents a few important details of the numerical implementation. Section IV presents modeling a nanotube-metal molecular junction. In Sec. V, we summarize and give an outlook of future work. Finally, mathematical details of our *ab initio* technique is presented in several Appendixes.

II. THEORETICAL FORMALISM: BOUNDARY CONDITIONS, ELECTRODES, AND DENSITY MATRIX

As mentioned above, to investigate properties of the molecular device such as that shown in Fig. 1 we will make use of the familiar DFT *ab initio* method[38,41,42] to describe the electronic degrees of freedom. The atomic cores are defined by standard norm-conserving nonlocal pseudopotentials.[49] To be specific, in this work we use a minimal *s*, *p* real space Fireball linear combination of atomic orbitals (LCAO) basis set[42] $\{\zeta_\mu(\mathbf{r}-\mathbf{R}_I)\}$ to expand the KS wave functions. Furthermore, we note that, because of the open boundary conditions, a real space technique is needed to calculate the Hamiltonian and effective potential within DFT. The use of a minimal basis set results in an efficient calculation and also acceptable accuracy as amply documented in the literature.[50,42,51,24] We note that systematic improvements may be achieved in LCAO basis sets[54] so as to give comparable accuracy to large basis set methods such as plane waves,[41] multigrids,[52] or wavelets.[53] The latter methods cannot be used in our approach because the computational requirements to construct the NEGF would be too large using such basis sets. To save space, we do not present these familiar DFT details. Suffice it to say that once the charge density is constructed, the rest of the DFT iterations is carried out in standard fashion which can be found in the DFT literature.[41,42,38]

In what follows, we focus on the novel parts of our formalism: (1) How to deal with an open therefore infinitely large device system and (2) How to calculate the charge distribution under external bias for an open system. The details of how to calculate the Hamiltonian operator in matrix form and the effective potential $V^{\text{eff}}(\mathbf{r})$, can be found in Appendix C.

A. Boundary conditions for the Kohn-Sham potential

The device boundary condition plays a crucial role in simulating transport through a molecular device. Essentially, the wave functions, and thus the electric current through the device, depend on the KS effective potential[22,30] of the entire device: $\Psi=\Psi[V^{\text{eff}}[\rho(\mathbf{r})]]$. For our problem, the accurate effective potential $V^{\text{eff}}[\rho(\mathbf{r})]$ should be constructed by calculating the charge distribution for the *open* system which is, actually, infinitely large because the electrodes extends to $z=\pm\infty$.

Approximations to the device potential $V^{\rm eff}[\rho(\mathbf{r})]$ may be made by modeling only the central simulation box (labeled c) of Fig. 1 as a finite cluster or as a supercell. If more and more atomic layers of the electrodes are added to the central box, the KS potential near the molecular region begins to mimic the correct potential which requires the electrodes to be infinitely long. However, the KS wave functions obtained this way have incorrect boundary conditions for quantum scattering and therefore cannot be used to calculate electric current through the device. For this reason, an extra quantum scattering calculation must be carried out after matching the finite cluster or supercell potential to perfect electrodes potentials.[22,27] This kind of indirect approach has limited applicability because there are no electron reservoirs to maintain a chemical potential difference across the device, and therefore, no external bias potential may be applied to the device.

To deal with *open* boundary conditions for the KS potential, we make a simple observation that the KS potential deep inside a solid surface is very close to the corresponding bulk KS potential. This fact leads to a screening approximation which forms a natural boundary condition for open device systems:

$$V^{\rm eff}(\mathbf{r})=\begin{cases} V_l^{\rm eff}(\mathbf{r})=V_{l,\rm bulk}^{\rm eff}(\mathbf{r}), & z\leqslant z_l, \\ V_c^{\rm eff}(\mathbf{r}), & z_l<z<z_r, \\ V_r^{\rm eff}(\mathbf{r})=V_{r,\rm bulk}^{\rm eff}(\mathbf{r}), & z\geqslant z_r, \end{cases} \tag{1}$$

where the planes $z=z_l$ and $z=z_r$ are the left and right limits of the central simulation box that describes the scattering region (see Fig. 1). The simulation box should be large enough so that these planes are sufficiently deep enough inside the surface of the electrode such that Eq. (1) holds.

The boundary condition in Eq. (1) naturally divides the device into a scattering region or center cell (c), left cells belonging the left electrode (l), and right cells belonging to the right electrode (r) [see Fig. 1]. The atomic structure in the left (and right) cells is required to be identical to that of the corresponding bulk system, so that that each electrode is described by an effective potential $V_{l/r,\rm bulk}^{\rm eff}(\mathbf{r})$. Clearly, the electrodes do not have to be the same: the left cells can be crystalline Al to simulate an Al electrode, while the right cells can be a perfect carbon nanotube to simulate a nanotube electrode. As such, $V_{l/r,\rm bulk}^{\rm eff}(\mathbf{r})$ is obtained by a separate ''electrode'' calculation,[55] described in the next subsection, and stored in a database. With this (l,c,r) division, only the effective potential within the scattering region, $V_c^{\rm eff}(\mathbf{r})$, needs to be updated at each iteration of the self-consistent KS equations.

There remains the difficulty of having to match the effective potential inside the scattering region to that outside, i.e., to ensure that Eq. (1) holds at z_l and z_r. While it is not straightforward to impose a boundary condition on the total KS potential $V_c^{\rm eff}(\mathbf{r})$ it is natural to apply matching boundary conditions to the Hartree potential $V_c^H(\mathbf{r})$ by solving the Poisson equation in real space as a boundary value problem with the following boundary conditions

$$\begin{aligned} V_c^H(\mathbf{r})\big|_{z_l}&=V_{l,\rm bulk}^H(\mathbf{r})\big|_{z_l}, \\ V_c^H(\mathbf{r})\big|_{z_r}&=V_{r,\rm bulk}^H(\mathbf{r})\big|_{z_r}, \end{aligned} \tag{2}$$

where $V_{l,\rm bulk}^H(\mathbf{r})\big|_{z_l}$ and $V_{r,\rm bulk}^H(\mathbf{r})\big|_{z_r}$ are the Hartree potentials of the equivalent bulk systems. We have used a multigrid technique to solve the Poisson equation in three-dimensional (3D) real space[56] to apply Eq. (2). The total KS potentials $V_{l/r,\rm bulk}^{\rm eff}(\mathbf{r})$ and $V_c^{\rm eff}(\mathbf{r})$ will then be equal at $z_{l/r}$ within the local density approximation of DFT, if the charge densities $\rho_c(\mathbf{r})$ and $\rho_{l/r,\rm bulk}(\mathbf{r})$ are equal at $z_{l/r}$. Again, this is indeed the case if $z_{l/r}$ is chosen far enough inside the electrode surface, which one can confirm numerically[57] during a simulation.

The above requirements on the effective potential, Eqs. (1),(2), reduce the infinitely large open device problem defined on all space, to a problem defined on the finite scattering region. This way, we only have to calculate charge density and effective potential inside the scattering region in order to solve the KS equations.

B. Electrode potential

In our model, each electrode consists of a collection of atoms at positions $\{\mathbf{R}_I\}$ in a unit cell which is repeated to $z=\pm\infty$. In order to apply the boundary conditions Eqs. (1),(2), we must first calculate $V_{l/r,\rm bulk}^{\rm eff}(\mathbf{r})$.

Each electrode unit cell can be associated with an LCAO basis $\{\zeta_z\}$. It is not difficult to confirm that the unit cell may always be chosen so that the Hamiltonian has the following tridiagonal form:

$$\begin{bmatrix} \ddots & \ddots & \ddots & & & \\ & h_{z,z-1} & h_{z,z} & h_{z,z+1} & & \\ & & h_{z,z-1} & h_{z,z} & h_{z,z+1} & \\ & & & \ddots & \ddots & \ddots \end{bmatrix}. \tag{3}$$

Here, $h_{z,z'}$ is itself a Hamiltonian matrix defined on unit cells labeled by the integers z and z'. The construction of the Hamiltonian matrix elements $h_{z,z'}$ is straightforward and is discussed in Appendix C. Using the Bloch ansatz

$$\Psi^k(z)=e^{ikz}\phi^k\equiv[\lambda^k]^z\phi^k, \tag{4}$$

Schrödinger's equation becomes

$$\begin{aligned} &[h_{z,z-1}[\lambda^k]^{-1}+h_{z,z}+h_{z,z+1}[\lambda^k]^{+1}]\phi^k \\ &\quad=E^k[s_{z,z-1}[\lambda^k]^{-1}+s_{z,z}+s_{z,z+1}[\lambda^k]^{+1}]\phi^k, \end{aligned} \tag{5}$$

where $s_{z,z'}$ represents the overlap matrix elements calculated between basis states in the z and z' unit cells. By choosing appropriate values of k, one can diagonalize the above equation in order to obtain the eigenvalues E^k and eigenstates ϕ^k.

The density matrix of the electrode is obtained by integrating over the Brillouin zone in the usual fashion:

$$\hat{\rho}=\int dk|\Psi^k\rangle f^{\rm eq}(E^k;\mu)\langle\Psi^k|,$$

where

$$f^{\mathrm{eq}}(E;\mu)\equiv\frac{1}{1+e^{-(E-\mu)/k_BT_e}}$$

is the equilibrium Fermi function for electrons of temperature T_e. The chemical potential μ is determined by the charge neutrality condition

$$\int dk f^{\mathrm{eq}}(E^k;\mu)=N,$$

where N the number of electrons in the unit cell. By constructing the charge distribution within the unit cell $\rho(\mathbf{r})=\hat{\rho}(\mathbf{r},\mathbf{r})$ the KS potential of electrodes $V^{\mathrm{eff}}_{l/r,\mathrm{bulk}}(\mathbf{r})$ can be updated and the KS equations solved self-consistently.

The electrode calculation provides the following information which are saved to an electrode database: the positions of the atoms in the unit cell $\{\mathbf{R}_{l/r}\}$, $V^{\mathrm{eff}}_{l/r,\mathrm{bulk}}(\mathbf{r})$, the Hartree potential on the boundary of the unit cell $V^{H}_{l/r,\mathrm{bulk}}(\mathbf{r})|_{z_{l/r}}$, the electrode Hamiltonian in the form of the coupling matrices $\{h_{l/r,l/r-1},h_{l/r,l/r},h_{l/r,l/r+1},\}$, the overlap matrix $\{s_{l/r,l/r-1},s_{l/r,l/r},s_{l/r,l/r+1}\}$, and the chemical potential $\mu_{l/r}$ which ensures that each electrode is charge neutral.

C. Density matrix of an open device system

Using the boundary conditions Eqs. (1),(2), the KS equations can be solved iteratively by constructing the charge distribution inside the device region $\rho_c(\mathbf{r})$ which in turn generates a new effective potential $V^{\mathrm{eff}}_c[\rho_c(\mathbf{r})]$. The charge distribution is conveniently calculated from the density matrix $\hat{\rho}$, which can be constructed in two ways, either by including all the eigenstates of the open device with the proper statistical weight, or from the nonequilibrium Green's function (NEGF) (Refs. 44,43,45) which is what we use.

To begin, we note that for LCAO fireball basis set[50,42] which we use in our model, the Hamiltonian matrix of the entire device including the infinitely long electrodes, can always be written into a tridiagonal form

$$\begin{bmatrix} h_{l,\infty} & h_{l,l+1} & 0 & 0 & 0 \\ h_{l,l-1} & h_{l,l} & h_{l,c} & 0 & 0 \\ 0 & h_{c,l} & h_{c,c} & h_{c,r} & 0 \\ 0 & 0 & h_{r,c} & h_{r,r} & h_{r,r+1} \\ 0 & 0 & 0 & h_{r,r-1} & h_{r,\infty} \end{bmatrix}. \tag{6}$$

Note this matrix is actually infinitely large due to the semi-infinite electrode Hamiltonians $h_{l,\infty}$ and $h_{r,\infty}$:

$$h_{l,\infty}\equiv\begin{bmatrix} \ddots & \ddots & \ddots & 0 \\ 0 & h_{l,l-1} & h_{l,l} & h_{l,l+1} \\ 0 & 0 & h_{l,l-1} & h_{l,l} \end{bmatrix}, \tag{7}$$

$$h_{r,\infty}\equiv\begin{bmatrix} h_{r,r} & h_{r,r+1} & 0 & 0 \\ h_{r,r-1} & h_{r,r} & h_{r,r+1} & 0 \\ 0 & \ddots & \ddots & \ddots \end{bmatrix}$$

which are derived from the electrode calculations. Similarly, one can also define the equivalent overlap matrices $s_{l,\infty}$ and $s_{r,\infty}$. In addition, applying a bias potential $\Delta V_{l/r}$ to an electrode simply entails a shift of the electrode potential in the following way:

$$V^{\mathrm{eff}}_{l/r,\mathrm{bulk}}(\mathbf{r})\leftarrow V^{\mathrm{eff}}_{l/r,\mathrm{bulk}}(\mathbf{r})+\Delta V_{l/r},$$

$$V^{H}_{c}(\mathbf{r})|_{z_{l/r}}\leftarrow V^{H}_{c}(\mathbf{r})|_{z_{l/r}}+\Delta V_{l/r},$$

$$h_{l/r,\infty}\leftarrow h_{l/r,\infty}+s_{l/r,\infty}\Delta V_{l/r}. \tag{8}$$

The Hamiltonian matrix (6) is diagonalized by the scattering states incident from the left electrode $\{\Psi^{k^n_l}\}$, the scattering states incident from the right electrode $\{\Psi^{k^n_r}\}$, as well as a discrete set of bound states $\{\Psi^{c^n}\}$. Once these eigenstates are calculated, one can construct the density matrix $\hat{\rho}$ by integrating their modular over the three sets of labels $\{k^n_l,c^n,k^n_r\}$,

$$\hat{\rho}=\sum_{c^n}|\Psi^{c^n}\rangle f^{c^n}\langle\Psi^{c^n}|+\int dE\left[|\Psi^{k^n_l}\rangle\frac{f^{k^n_l}}{v^{k^n_l}}\langle\Psi^{k^n_l}|+|\Psi^{k^n_r}\rangle\times\frac{f^{k^n_r}}{v^{k^n_r}}\langle\Psi^{k^n_r}|\right], \tag{9}$$

where $v^{k^n_l}\equiv\partial E/\partial k^n_l$ and $v^{k^n_r}\equiv\partial E/\partial k^n_r$ are the group velocities corresponding to the k^n_l and k^n_r channels of the electrodes. These expressions give a practical way to construct the density matrix once the scattering states and bound states are known. Although the scattering eigenstates can be efficiently calculated,[40] as shown in Appendix D it is, however, rather difficult to calculate the bound states. Therefore, we construct density matrix using the nonequilibrium Green's function[43–45] $G^<$

$$\hat{\rho}=-\frac{i}{2\pi}\int dE G^<(E), \tag{10}$$

where

$$G^<=G^R\Sigma^<[f^{k^n_l},f^{k^n_r}]G^A \tag{11}$$

and $G^{R/A}$ is the retarded/advanced Green's function of the device (for their calculation, see Appendix A). The quantity $\Sigma^<[f^{k^n_l},f^{k^n_r}]$ represents injection of charge from the electrodes[44] and can be written in terms of the self-energies $\Sigma^L_{l,l}$ and $\Sigma^R_{l,l}$ due to coupling to the left and right electrodes (for their calculation, see Appendix B):

$$\Sigma^<[f^{k^n_l},f^{k^n_r}]=-2i\,\mathrm{Im}(f^{k^n_l}\Sigma^l_{l,l}+f^{k^n_r}\Sigma^r_{r,r}). \tag{12}$$

Of course, the density matrix calculated using the NEGF Eq. (10) is exactly equivalent to that calculated using the eigenstates by Eq. (9).

It remains to specify the distribution functions $\{f^{k^n_l},f^{c^n},f^{k^n_r}\}$. In the equilibrium situation where the electrochemical potentials of the left and right electrodes are equal

$$\mu^*=\mu_l+\Delta V_l=\mu_c=\mu_r+\Delta V_r, \tag{13}$$

the distribution functions are given by the equilibrium Fermi distribution

$$f^{k_l^n}(E;\mu_l+\Delta V_l)=f^{c^n}(E;\mu_c)$$
$$=f^{k_r^n}(E;\mu_r+\Delta V_r)=f^{\mathrm{eq}}(E,\mu^*). \quad (14)$$

We note that, in clear contrast to the study of closed systems (e.g., finite cluster or supercells), the electrochemical potentials of an open system $\mu_{l/r}+\Delta V_{l/r}$, are known *a priori* from the ''electrode'' calculation described above.

Finally, we discuss the distribution functions in the nonequilibrium situation when $\mu_l+\Delta V_l \neq \mu_r+\Delta V_r$. First of all, the distribution functions of the electrodes (and reservoirs) can be approximated[44] as

$$f^{k_l^n}(E;\mu_l+\Delta V_l)=f^{\mathrm{eq}}(E;\mu_l+\Delta V_l),$$
$$f^{k_r^n}(E;\mu_r+\Delta V_r)=f^{\mathrm{eq}}(E;\mu_r+\Delta V_r). \quad (15)$$

This way, we have neglected any influence that the device scattering region has on the distribution functions of the electrodes and reservoirs. This is a reasonable assumption for our purposes and is commonly used in quantum transport literature.[44] Next, the distribution of the bound states is assumed to be $f^{c^n}=f^{\mathrm{eq}}(E;\mu_c)$ where $\mu_c=\mu_l+\Delta V_l$ or $\mu_c=\mu_r+\Delta V_r$. The two choices are equivalent if there are no bound states in the interval $[\mu_l+\Delta V_l,\mu_r+\Delta V_r]$, which can be confirmed numerically. To end this section, we emphasize that given the distribution functions $\{f^{k_l^n},f^{c^n},f^{k_r^n}\}$, the self-consistent solution of the KS equations is essentially exact (within DFT) for open device systems, if the size of the simulation box is chosen large enough, which we confirm numerically during a calculation.

III. NUMERICAL PROCEDURE

In the next subsection we discuss the procedure of evaluating the energy integration in Eq. (10) for computing charge density. The use of the NEGF, as opposed to the eigenstates of the open system, to construct charge density is the most important and novel point of our *ab initio* technique. Once the charge density is obtained, one can then perform the usual DFT self-consistent iterations. We will also present procedures of calculating physical quantities and discuss some numerical results. Finally, the calculations of retarded Green's function G^R and the self-energy are included in Appendixes A and B.

A. Calculation of charge density

In order to calculate charge density from Eq. (10), we must perform the energy integration over the density of states (DOS) which is the integrand. The charge density must be obtained very accurately, otherwise the self-consistent DFT analysis would not produce the correct results.

From the point of view of constructing the charge density $\rho(\mathbf{r})$, the essential difference between the NEGF $G^<$ and the retarded Green's function G^R, is that $G^<$ contains information about the distribution function[43] through the injected charge $\Sigma^<[f^{k_l^n},f^{k_r^n}]$. In other words, the NEGF tells us how to fill the states of an open device system under bias, according to Eq. (10). In the equilibrium situation without bias, i.e., when the chemical potentials of the electrodes are equal, $G^<$ is reduced to a simple form[43,45]

$$\mathrm{Im}[G^<(E)]=-2f^{\mathrm{eq}}(E)\mathrm{Im}[G^R(E)]. \quad (16)$$

Importantly, this expression remains true even for situations where the electrochemical potentials are different — so long as

$$f^{k_l^n}(E)=f^{k_r^n}(E)=1. \quad (17)$$

This is simply because when Eq. (17) is satisfied, there is no additional information in the distribution functions $f^{k_l^n}$ and $f^{k_r^n}$.

Therefore, we can split the integral of Eq. (10) into two terms: an ''equilibrium'' contribution $\hat{\rho}^{\mathrm{eq}}$, where $f^{k_l^n}(E)=f^{k_r^n}(E)=1$ and a ''nonequilibrium'' contribution $\hat{\rho}^{\mathrm{neq}}$, where Eq. (17) is not satisfied. The density matrix can be written

$$\hat{\rho}=\hat{\rho}^{\mathrm{eq}}+\hat{\rho}^{\mathrm{neq}}, \quad (18)$$

where

$$\hat{\rho}^{\mathrm{eq}}\equiv-\frac{1}{\pi}\mathrm{Im}\left[\int_{-\infty}^{\mu_{\min}}dEG^R(E)\right], \quad (19)$$

$$\hat{\rho}^{\mathrm{neq}}\equiv-\frac{i}{2\pi}\int_{\mu_{\min}}^{\mu_{\max}}dEG^<(E), \quad (20)$$

where $\mu_{\min}\equiv\min(\mu_l+\Delta V_l,\mu_r+\Delta V_r)$, $\mu_{\max}\equiv\max(\mu_l+\Delta V_l,\mu_r+\Delta V_r)$. In Eq. (19), we have assumed that the electrons are at $T_e=0$ so that the distribution functions are step functions, but Eq. (19) can easily be rewritten for arbitrary distribution functions $\{f^{k_l^n},f^{k_r^n}\}$.

The equilibrium charge contribution $\hat{\rho}^{\mathrm{eq}}$ is related to the retarded Green's function $G^R(E)$ which can be analytically continued into the complex energy plane.[58] Thus, the integration in Eq. (19) can be evaluated along a suitable contour in the complex plane. For concreteness, we have chosen the semicircular contour illustrated in Fig. 2 where $E_{\min}$ is chosen sufficiently low so that it is lower than the lowest eigenvalue of H. The integration itself is accomplished using a Gaussian quadrature of the parameter $0<\theta<\pi$. The result converges rapidly as the number of quadrature points is increased (typically 30 quadrature points are enough). This contour integration has tremendous computational advantages because the DOS is very smooth away from the real axis, thus avoiding the many van Hove singularities in the DOS. In Fig. 3, we show the DOS and band structure as functions of energy for a perfect carbon chain with a four-atom unit cell; the inset shows the integrated DOS along a complex contour (see Fig. 2). Clearly, the van Hove singularities (peaks in DOS in Fig. 3) will make it tremendously difficult to integrate the DOS along the real axis while the DOS along the complex contour is very smooth. Indeed, as

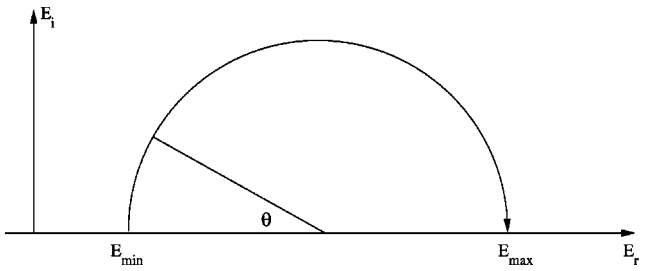

FIG. 2. Analytical continuation of G^R into the complex energy plane (E_r, E_i). The equilibrium charge contribution is calculated by exploiting the analytical properties of G^R. The integral around the semicircle C is equal to the integral along the real axis R between $E_{\min}$ and $E_{\max}$. The equilibrium charge contribution is calculated by choosing a sufficiently low value of $E_{\min}$ and $E_{\max}=\min(\mu_l+V_l, \mu_r+V_r)$.

shown in the inset of Fig. 3, the total integrated DOS is 16 when the contour integration is completed, which is the number of valence electrons in the four-atom unit cell. We also note that such a complex contour automatically includes the charge contribution from any bound states below $\mu_{\min}$, which would appear as δ functions along the real axis. The contour integration is most important for any self-consistent analysis, because, as opposed to simple transport calculations, one must integrate over the entire spectrum (including bound states) which would normally require a prohibitively large number of evaluations of $G^<$ to reach a reasonable accuracy for constructing the charge density.

The nonequilibrium charge contribution is evaluated using Eq. (20). In energy ranges where Eq. (17) is not satisfied, $\mathrm{Im}[G^<] \neq -2f^{\mathrm{eq}}(E)\mathrm{Im}[G^R]$, and the DOS must be calculated from the NEGF Eq. (11). Because $G^A(E)$ is nonanalytic above the real axis while $G^R(E)$ is nonanalytic below the real axis, $G^<(E)$ is only analytic along the real axis. It is

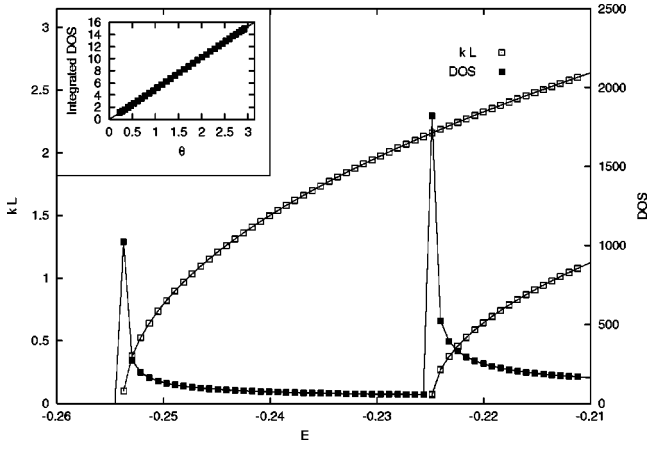

FIG. 3. The density of states (DOS, solid squares) and band structure (kL vs E, empty squares) versus energy, for a perfect carbon atomic chain with a four-atom unit cell (unit cell length L). The peaks in DOS are the van Hove singularities at the band edges. The inset shows the integrated density of states along a complex contour versus the contour variable θ. DOS is very smooth along the complex contour and the integral converges with a small number of Gaussian quadrature points.

therefore impossible to make use of a contour integral to evaluate Eq. (20) and thus the nonequilibrium charge must be calculated along the real axis directly. Hence,

$$\hat{\rho}^{\mathrm{neq}} = -\frac{i}{2\pi}\int_{\mu_{\min}}^{\mu_{\max}} dE\, G^R \Sigma^< [f^{k_l^n}, f^{k_r^n}] G^A. \tag{21}$$

So long as there are no band edges in the interval $[\mu_l + \Delta V_l, \mu_r + \Delta V_r]$, the energy integration will be smooth along the real axis and a Gaussian quadrature is found to converge with a small number of evaluations of $G^<$. As a check to the contour numerical procedure, for an infinitely long perfect carbon chain where there is no bound state, we have calculated charge density using both Eqs. (10) and (9) and obtained exactly the same results.

B. Evaluating physical quantities

By including the semi-infinite electrodes as self-energies, as in Eq. (A3), and only evaluating the density matrix near the central cell, information about the system outside the central cell is discarded. However, if the central cell is chosen large enough, the density at the edge of the central cell will relax to the bulk value, and changes to physical quantities will be due solely to changes of the state of the device inside the internal cell c. Thus, changes in extensive physical quantities such as the band-structure energy or number of electrons (or changes in them) may be evaluated by averaging over the central cell. This average is calculated by performing a trace over the indices of the density matrix corresponding to the central cell. For example, the band-structure energy in our formalism is given by

$$E_{\mathrm{BS}} = \mathrm{Tr}_c[\rho H] = \rho_{c,l}h_{l,c} + \rho_{c,c}h_{c,c} + \rho_{c,r}h_{r,c}. \tag{22}$$

Since changes in physical quantities may be calculated, one can also calculate the Hellmann-Feynman forces $-\partial E/\partial \mathbf{R}_I$ and optimize the atomic coordinates of the *open* system under the influence of external fields. We will not report quantum molecular dynamics simulations for open systems under bias in this work and leave that topic for the future.[59]

The transport properties we are interested in this work is the electric current which is evaluated using the Landauer formula

$$I = \frac{2e}{h}\int_{\mu_{\min}}^{\mu_{\max}} dE\, (f^{k_l^n} - f^{k_r^n}) T(E), \tag{23}$$

where $T(E)$ is the transmission probability and is given by[43]

$$T(E) = 4\,\mathrm{Tr}[\mathrm{Im}(\Sigma_{l,l}^l) G_{l,r}^R \,\mathrm{Im}(\Sigma_{r,r}^r) G_{r,l}^A]. \tag{24}$$

It is emphasized that, since the current is calculated from a self-consistent analysis, the functions inside the trace in Eq. (24) are all functions of bias potentials $\Delta V_{l/r}$ so that gauge invariant nonlinear *I-V* curves are obtained. The importance of gauge invariance in a nonlinear transport theory has been emphasized by Büttiker and co-workers[60–63] and we refer interested readers to their original contributions.

At equilibrium, the current is proportional to the conductance G,

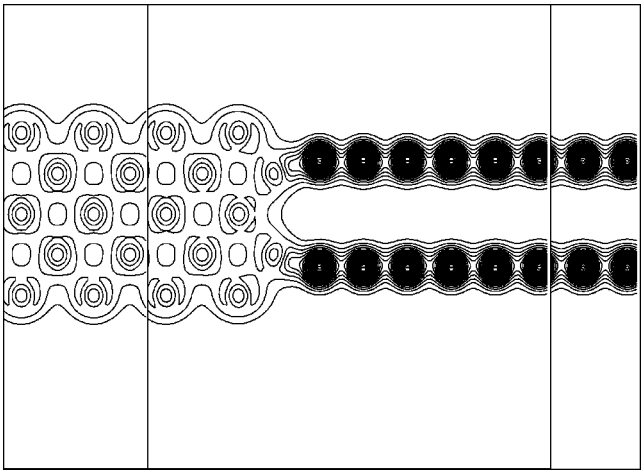

FIG. 4. Charge density contours of the carbon nanotube-metal interface of Fig. 1 at equilibrium. The contours of the bulk lead match that of the device at the edges of the device region.

$$I = G(\mu) \times (\mu_l - \mu_r) \tag{25}$$

which is evaluated at the Fermi level of the device

$$G(\mu) = \frac{2e^2}{h} T(\mu). \tag{26}$$

Finally, we comment that, within linear response, formulas may also be derived for the electrochemical capacitance,[60,23] the ac response coefficients,[60] and nonlinear conductance coefficients.[62,64] We leave the discussion of these linear response coefficients for atomic devices for the future.

C. Numerical validation

As mentioned above, for an open system without bound states (such as a perfect atomic chain), its transmission coefficient and DOS can be calculated by the scattering states,[40] or by Green's functions using Eq. (24). We have confirmed that exactly the same numerical values are obtained from these two approaches for all the systems we studied. Because the scattering state calculation is completely independent from the Green's function calculation,[40] this is a very strong test which validates the numerical procedure presented above, including the self-energy calculation (Appendix B), the contour integration, and the nonorthogonal Green's function formalism (Appendixes A,C).

A key ingredient of our formalism is the implementation of the screening approximation by imposing Eqs. (1),(2) on the KS effective potentials. However, no such restriction is placed on the charge density which we computed self-consistently from the NEGF. Indeed, for all the systems we have checked, a perfect match of charge density at $z_{l/r}$ is achieved by including a few layers of bulk electrode within the central cell. Figure 4 shows the equilibrium charge density $\rho(\mathbf{r})$ along a cross section of the xz plane for a carbon nanotube in contact with an Al(100) electrode (see Fig. 1). The high quality matching was also obtained for a C_{60} device[39] and several other molecular device systems we have studied.[40] Since the potential is uniquely determined by the charge distribution, this nontrivial result is strong evidence that the central cell is chosen large enough such that the potential is effectively screened, and therefore relaxes to the bulk value at the boundary.

IV. TRANSPORT THROUGH A CARBON NANOTUBE-METAL INTERFACE

In this section, we report our analysis on the transport properties of a single wall armchair carbon nanotube in contact with an Al electrode, shown in Fig. 1 where a semi-infinite nanotube is in contact with a semi-infinite Al electrode. Carbon nanotubes are either metals or semiconductors depending on their helicity, therefore they provide a very exciting possibility of forming an all carbon nanotube-based molecular electronic system. So far a considerable amount of experimental[48,10,9,8,65,66] and theoretical[67,15,14,68–71,21,66] effort has been devoted to understand the nanotube physics.[66] We refer interested readers to Ref. 66 for detailed discussions of other properties nanotubes and we will focus on presenting the transport properties of the nanotube-metal interface.

The most basic question concerning nanotube electronics is its conductance. For perfect single wall armchair nanotubes which are *infinitely* long, it is well known[72,73] that there are two states crossing the Fermi level of the nanotube. Therefore, for these ideal tubes the equilibrium conductance should be[66] $G = 2G_0$, where $G_0 = 2e^2/h$ is the conductance quanta. For infinitely long nanotubes with defects, the conductance is slightly influenced by scattering due to the defects, but $G \sim 2G_0$ is still maintained as predicted by theory.[27,28] To the best of our knowledge, however, experimental measurements of nanotube conductance have never found a $2G_0$ conductance up to now. In fact, most measurements report two orders of magnitude smaller values due, presumably, to the poor nanotube-electrode contacts. From this perspective, it is extremely interesting that a recent measurement, reported by Frank *et al.*,[48] showed $G \approx G_0$ by dipping a multiwall nanotube into a liquid metal repeatedly. Their measured[48] conductance is therefore half of the ideal theoretical value.[72,73] Clearly, the theoretical value of $2G_0$, which is only true for infinitely long metallic nanotubes, cannot explain the experimental data. To understand this discrepancy, Choi and co-workers reported[28] a plane wave *ab initio* calculation of an armchair nanotube in contact with a jellium electrode. Their analysis showed that there is considerable back scattering due to the nanotube-jellium contact. In particular, the π-band incident electron suffers strong scattering and its contribution to conductance is almost completely inhibited,[28] while the π^* band does not suffer back scattering and therefore it is its contribution which gave a G_0 conductance value. This result gives a plausible explanation to the experimental findings.[48]

To further investigate this problem for the case where a nanotube is in contact with an atomic electrode (as opposed to jellium electrode), and to predict the *I-V* curves of such an interface, we have studied the nanotube-metal interface shown in Fig. 1 using our NEGF-DFT technique presented previously. The system consists of a semi-infinite and perfect

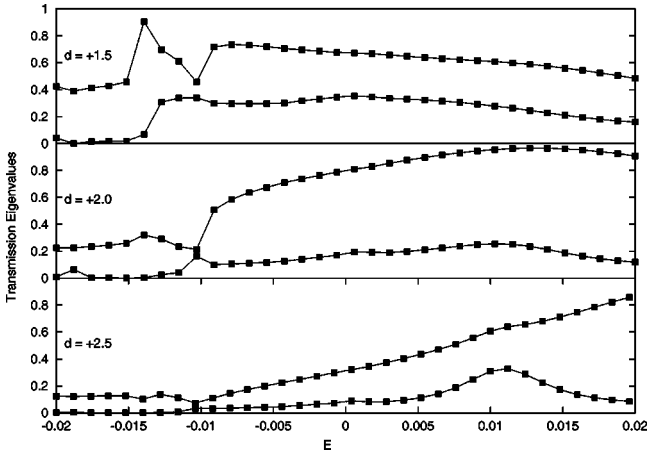

FIG. 5. The transmission eigenvalues (filled squares) of the two eigenmodes for the nanotube-metal interface as a function of electron energy. Each eigenmode contributes less than unity to the total transmission coefficient, but one contributes more than the other. The three panels correspond to different nanotube-metal junction distance d. Energy is normalized such that the Fermi level is at $E=0$. The total transmission coefficient (open squares) at Fermi energy is ~ 1 in unit of $G_0 \equiv 2e^2/h$ for the upper two panels and becomes much smaller when d is large.

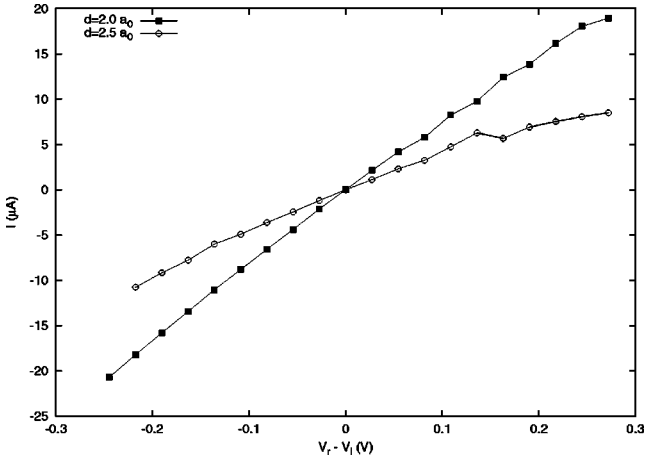

FIG. 6. The I-V curve for the nanotube-metal interface at $d=2$ and 2.5 a.u.. The result is obtained by fixing bias $V_l=0$ and varying V_r from negative to positive. The I-V curves are essentially linear with a slope $\sim G_0$ for $d=2$ a.u., and $\sim 0.39G_0$ for $d=2.5$ a.u., at small bias voltages.

single wall (4,4) nanotube[66] which is in contact with a semi-infinite Al electrode. The Al electrode is represented by slabs of bulk Al (100) with a finite cross section. We study the ideal situation where no structural relaxation is allowed. Therefore the nanotube-metal junction is characterized by the contact distance d, which is the distance between the left most ring of carbon atoms and the right most layer of the Al atoms (see Fig. 1), which we vary as a control parameter.

Our analysis shows that there are two transmission eigenvectors which connect the two sides of the nanotube-electrode interface. This is consistent with the fact that a perfect and infinitely long nanotube has two states at its Fermi level. As usual,[46,47] the transmission eigenvectors and eigenvalues are obtained by diagonalization of the scattering matrix which we calculated from the NEGF via the Fisher-Lee relationship.[74,44] The two transmission eigenvalues T_1 and T_2 are plotted in Fig. 5 as a function of energy E for three values of junction distance $d=1.5,2.0,2.5$ a.u., where E is normalized so that $E_F=0$. The total transmission coefficient is therefore $T=T_1+T_2$, and this gives equilibrium conductance at Fermi energy to be $G=1.01G_0, 0.98G_0, 0.39G_0$, for the three d's, respectively. Our results suggest that both transmission eigenvectors contribute substantially to the conductance although one contributes more than the other, and there are also substantial back scattering at the interface making each transmission eigenvalues less than one. We believe the difference between the two transmission eigenvectors is related to the relative shifts of the carbon nanotube π and π^* bands which has been discussed in Ref. 28. The fact that they happen to add up to give $G \approx G_0$ is indeed interesting, and is true for a range of values of d. This result is thus in qualitative agreement with those of the nanotube-jellium interface.[28] Furthermore, our results suggest that the junction distance d plays an important role in controlling the interface transparency. This is understandable because d directly controls charge transfer between the two sides of the interface thereby determines the Fermi level alignment.

Finally, Fig. 6 shows the I-V curve for this system at $d=2$ and 2.5 a.u. To obtain this result, we fixed bias $V_l=0$ and varied V_r from negative to positive. The I-V curves are essentially linear with a slope $\sim G_0$ for $d=2$ a.u., and $\sim 0.39G_0$ for $d=2.5$ a.u., at small bias voltages. These results are consistent with the equilibrium conductance discussed in the last paragraph. The I-V curves showed a slight rectification which is due to the asymmetry across the interface. In contrast, the I-V curves for a C_{60} molecular junction were found to be quite nonlinear at similar range of bias voltages.[39] Our results, together with that of Ref. 28, allows us to conclude that the equilibrium conductance of a nanotube-metal interface should be $\sim G_0$ instead of $2G_0$, due to back scattering of the interface.

V. SUMMARY

In this paper, we have presented an *ab initio* technique to simulate quantum transport through open coherent quantum conductors. The novelty of this technique lies in constructing the electronic charge density via the nonequilibrium Green's functions, instead of using eigenstates of the conductor, with the help of a screening approximation which reduces the infinitely large problem to a finite calculation in the scattering region. The construction of the charge density from NEGF is facilitated by the analytic continuation technique which drastically reduces the computation effort. Because our DFT analysis is based on a real space technique with the Hartree potential solved on a real space grid, our technique allows simulations of devices with different electrodes (e.g., one carbon and the other aluminum), with bias as well as gate potentials.[39]

We have provided many results which clearly demonstrated the power of our technique, and in particular we have

simulated transport properties of a carbon nanotube-metal interface. We found that due to interface back scattering, the two transmission eigenvectors each contribute a transmission coefficient which is smaller than unity, with the total $\sim G_0$ for a range of the distance between the nanotube and the electrode. This is consistent with the nanotube-jellium results obtained before,[28] and is also consistent with the experimental measurements of Frank *et al.*[48] In this regard, we caution that the experiments were carried out on multiwall nanotubes while the theory is on single wall tubes.

Many further analyses of molecular nanoelectronics can be carried out using the technique presented here. Not only quantum transport properties including *I-V* curves can be predicted from first principles, but also structural analysis of open boundary nanodevices under external fields. The latter can be simulated with quantum molecular dynamics within our NEGF-DFT formalism.[59] Clearly, molecular electronic device systems with more than two electrodes can also be readily simulated within our formalism. From a numerical computation point of view, our method is easily parallelizable. More importantly, because we use a nonorthogonalized LCAO fireball basis set which has a finite range, our method can be made to scale as $O(N)$. We hope to report these developments in a future publication.

ACKNOWLEDGMENTS

We gratefully acknowledge many useful discussions with Dr. Gianni Taraschi on real space DFT techniques, with Professor Peter Grütter on SPM experimental methods, with Brian Larade and Hatem Mehrez on the detailed formulation of our NEGF-DFT formalism, and with Dr. B.G. Wang on theoretical issues related to nonequilibrium Green's functions. We gratefully acknowledge financial support from NSERC of Canada and FCAR of Quebec (H.G.) and RGC Grant No. HKU 7115/98P from the Hong Kong SAR (J.W.). J.T gratefully acknowledges financial support from NSERC.

APPENDIX A: GREEN'S FUNCTIONS OF A TWO PROBE DEVICE

In this appendix, we present expressions for the retarded Green's function. From Eq. (11), $G^<$ may be calculated once the retarded Green's function G^R is known. The calculation of G^R in a tight-binding basis set is well known[44] and we write down necessary formula for the sake of completeness and ease of presentation.

Expanding G^R in terms of the real space basis set using

$$G^R(\mathbf{r},\mathbf{r}') = |\zeta_\mu(\mathbf{r})\rangle G^R_{\mu\nu}\langle\zeta_\nu(\mathbf{r}')|, \tag{A1}$$

leads to the following equation for $G^R_{\mu\nu}$:

$$\lim_{\eta\to 0}[(E+i\eta)S_{\mu\nu'} - H_{\mu\nu'}]G^R_{\nu'\nu} = \delta_{\mu\nu}. \tag{A2}$$

To calculate the charge distribution of the scattering region of the device (see Fig. 1), we only need the components of density matrix in which the basis states have support inside the central cell. Namely, we only have to worry about those basis orbitals which extend into the central cell. Therefore we need to calculate a submatrix of $G^R_{\mu\nu}$ which corresponds to the central cell. As shown in Refs. 44, the central cell retarded Green's function has a very simple form in LCAO orbital space

$$g_{CC} = \begin{bmatrix} h^E_{l,l} - \Sigma^l_{l,l} & h^E_{l,c} & 0 \\ h^E_{c,l} & h^E_{c,c} & h^E_{c,r} \\ 0 & h^E_{r,c} & h^E_{r,r} - \Sigma^r_{r,r} \end{bmatrix}^{-1}, \tag{A3}$$

where $h^E_{i,j} \equiv (E+i\eta)s_{i,j} - h_{i,j}$ and $\Sigma^l_{l,l}$ and $\Sigma^r_{r,r}$ are the self-energies due to coupling to the left and right electrodes, respectively. In terms of the surface Green's functions $g_{l,\infty} \equiv [(E+i\eta)s_{l,\infty} - h_{l,\infty}]^{-1}$ and $g_{r,\infty} \equiv [(E+i\eta)s_{r,\infty} - h_{r,\infty}]^{-1}$, the self-energies can be written[75]

$$\begin{aligned} \Sigma^l_{l,l} &\equiv h^E_{l,l-1} g_{l,\infty} h^E_{l,l+1}, \\ \Sigma^r_{r,r} &\equiv h^E_{r,r-1} g_{r,\infty} h^E_{r,r+1}. \end{aligned} \tag{A4}$$

We calculate the self-energies using a procedure described in the next subsection and the Green's function is then obtained by direct matrix inversion of Eq. (A3). We note that efficient techniques of inverting large sparse matrices in $O(N)$ operations exist.[76]

APPENDIX B: SELF-ENERGIES

In this appendix we derive the necessary expressions for computing the self-energies. There are many methods in the literature for evaluating self-energy due to coupling to electrodes.[44,75] For self-consistent calculations, an efficient method must be used because of the many iteration steps in the DFT procedure. We have chosen to extend a method proposed by Sanvito *et al.*[77] because this method allows for a direct evaluation of the self-energy and it does not rely on a finite smearing parameter η which is employed in most iterative methods.[75]

The method of Ref. 77 is valid for situations where the coupling matrices $\{h^E_{l,l-1}, h^E_{l,l+1}, h^E_{r,r-1}, h^E_{r,r+1}\}$ are nonsingular so as to have a simple inverse. For our *ab-initio* analysis where the range of interaction is fixed by the support of the basis orbitals and not by a semiempirical parametrization, these matrices may be singular. Here we describe a direct extension to the technique of Ref. 77 to deal with singular matrices.

Consider an infinitely long perfect electrode described by the infinite chain $\{h^E_{z,z-1}, h^E_{z,z}, h^E_{z,z+1}\}$ as in Eq. (3). By diagonalizing Eq. (5), we solve[40] the Bloch states and classify them into right-moving and left-moving groups according to their group velocities,[40] denoting them as $\{\phi^{l/r}\}$. We also calculate their duals defined by

$$\tilde{\phi}^{l/r}_i \equiv \phi^{l/r}_j \langle \phi^{l/r} | \phi^{l/r} \rangle^{-1}_{ji}. \tag{B1}$$

Following Sanvito *et al.*,[77] we make the following ansatz for the retarded Green's function of an infinitely long perfect electrode:

$$G^R_{\rm bulk}(z,z')=\begin{cases} g^+_{\rm bulk}(z,z') & z>z', \\ g^-_{\rm bulk}(z,z') & z<z', \end{cases} \tag{B2}$$

where

$$g^+_{\rm bulk}(z,z')\equiv\sum_r |\phi^r\rangle[\lambda^r]^{z-z'}\langle\tilde{\phi}^r|V,$$
$$g^-_{\rm bulk}(z,z')\equiv\sum_l |\phi^l\rangle[\lambda^l]^{z-z'}\langle\tilde{\phi}^l|V. \tag{B3}$$

The index z, as before, is an integer labeling the unit cells of the electrode and the quantity V is a matrix to be specified below. Note that the retarded boundary condition is satisfied because of the choice of phase $\lambda^{z-z'}$. The quantity V was also given in Ref. 77 in a form that is valid when the coupling matrices are nonsingular. By substituting the ansatz (B2) and multiplying by $H-ES$ using Eq. (3), it is straightforward to prove that the following choice of V will make the electrode Green's function (B2) satisfy the Green's function equation (A2),

$$V\equiv\left[\sum_L h^E_{z,z-1}|\phi^l\rangle[\lambda^l]^{-1}\langle\tilde{\phi}^l|+h^E_{z,z} + \sum_r h^E_{z,z+1}|\phi^r\rangle\lambda^r\langle\tilde{\phi}^r|\right]^{-1}. \tag{B4}$$

Note that this result reduces to the form given in Ref. 77 when the coupling matrices are nonsingular.

With the Green's function of an infinitely long perfect electrode calculated, as in Eq. (B2), we can now calculate the left surface Green's function $g_{l,\infty}$, which is needed in Eq. (A4). By its definition and using Eq. (7), $g_{l,\infty}$ satisfies

$$\begin{bmatrix} \ddots & \ddots & \ddots & \\ & h^E_{l,l-1} & h^E_{l,l} & h^E_{l,l+1} \\ & 0 & h^E_{l,l-1} & h^E_{l,l} \end{bmatrix} g_{l,\infty}=I_{l,\infty}. \tag{B5}$$

We form $g_{l,\infty}$ by adding a sum of left moving Bloch states to the bulk Green's function of the left electrode $G^R_{l,\rm bulk}$:

$$g_{l,\infty}(z,z')=G^R_{l,\rm bulk}(z,z')+\Delta_{l,\infty}(z), \tag{B6}$$

where

$$\Delta_{l,\infty}(z)\equiv\left[\sum_l |\phi^l\rangle(\lambda^l)^{z-c+2}\langle\tilde{\phi}^l|\right]\delta_{l,\infty} \tag{B7}$$

for $z<c-1$. Substituting Eq. (B7) into the last row of Eq. (B5) yields the following equation for $\delta_{l,\infty}$:

$$\sum_l [h^E_{l,l-1}(\lambda^l)^{-1}+h^E_{l,l}]|\phi^l\rangle\langle\tilde{\phi}^l|\,\delta_{l,\infty} = h^E_{l,l+1}g^+_{l,\rm bulk}(c-1,c-2), \tag{B8}$$

thus defining the surface Green's function $g_{l,\infty}$ in Eq. (B6) and the self-energy

$$\Sigma^l_{l,l}=h^E_{l,l-1}g_{l,\infty}(c-2,c-2)h^E_{l,l+1}. \tag{B9}$$

By precisely the same procedure, one can derive $g_{r,\infty}$ which then gives $\Sigma^r_{r,r}$ from Eq. (A4). As a validation to our closed form (B9) for the self-energies, we have calculated the self-energies using a transfer matrix technique[70,75] and obtained exactly the same numerical results.

APPENDIX C: CALCULATION OF HAMILTONIAN MATRIX ELEMENTS

Some details concerning the calculation of Hamiltonian matrix elements are presented in this appendix.[78,51] We use a minimal sp basis set to expand the electronic wave functions. Following Sankey and Niklewski,[50] we used fireball pseudoatomic orbitals which are solutions to the radial Schrödinger equation derived from the pseudopotential.[49] By expanding all quantities on a real space grid, one may develop a fully self-consistent solution to the KS equations.[42] Our technique is similar to that of Ref. 42, except that the solution of the Poisson equation is performed and the matrix elements of the effective potential $\langle V^{\rm eff}(\mathbf{r})\rangle_{\mu\nu}$ are calculated in real space for the piecewise continuous function $V^{\rm eff}(\mathbf{r})$.

The KS Hamiltonian has the following form:

$$H=\left[-\frac{\nabla^2}{2}+V^{\delta H}(\mathbf{r})+V^{\rm NA}(\mathbf{r})+V^{\rm xc}(\mathbf{r})\right]\delta(\mathbf{r}-\mathbf{r}') + V^{\rm NL}(\mathbf{r},\mathbf{r}'). \tag{C1}$$

Here $V^{\rm NA}(\mathbf{r})$ represents the local pseudopotential screened by the addition of charge density of the neutral isolated atoms[50] $\rho^{\rm NA}(\mathbf{r})$; $V^{\delta H}(\mathbf{r})$ is a screened Hartree potential which solves the corresponding Poisson equation

$$\nabla^2 V^{\delta H}(\mathbf{r})=-4\pi[\rho(\mathbf{r})-\rho^{\rm NA}(\mathbf{r})]. \tag{C2}$$

Multiplying by two LCAO basis states $\zeta_\mu(\mathbf{r}-\mathbf{R}_I)$ and $\zeta_\nu(\mathbf{r}-\mathbf{R}_J)$ and integrating over $d\mathbf{r}$ and $d\mathbf{r}'$ leads to the standard tight-binding matrix representation $H_{\mu\nu}$. One may derive general formulas for the kinetic energy, overlap, nonlocal pseudopotential and local pseudopotential matrix elements between two states of arbitrary angular momenta $(l_\mu m_\mu)$ and $(l_\nu m_\nu)$.[50,78] These involve integrals that may be pretabulated and stored in the database.

We solve the Poisson equation in the ''electrode'' calculation using a FFT technique. For open device systems, however, the potential must satisfy boundary condition Eq. (2). Hence we solve Eq. (C2) with a multigrid technique[56] directly in real space. The boundary conditions in the transverse direction may either be homogeneous or periodic. A gate potential V_g (see Fig. 1) can also be applied which capacitively couples to the device, it simply provides a boundary condition to $V^{\delta H}(\mathbf{r})$. Once $V^{\delta H}(\mathbf{r})$ is obtained, the exchange-correlation potential $V^{\rm xc}[\rho(\mathbf{r})]$ is added to it. By applying Eq. (1), the real-space part of the effective potential $V^{\rm eff}(\mathbf{r})$ is therefore known and is in a form of piecewise continuous function, as in Eq. (1).

The matrix elements of $V^{\rm eff}(\mathbf{r})$ are thus obtained as a sum of integrals over the real space grid:

$$\langle V^{\rm eff}\rangle_{\mu\nu}=\int_{\Omega_l} d\mathbf{r}\zeta_\mu(\mathbf{r}-\mathbf{R}_I)V^{\rm eff}_{l,\rm bulk}(\mathbf{r})\zeta_\nu(\mathbf{r}-\mathbf{R}_J)+\int_{\Omega_c} d\mathbf{r}\zeta_\mu(\mathbf{r}-\mathbf{R}_I)V^{\rm eff}_{c}(\mathbf{r})\zeta_\nu(\mathbf{r}-\mathbf{R}_J)+\int_{\Omega_r} d\mathbf{r}\zeta_\mu(\mathbf{r}-\mathbf{R}_I)V^{\rm eff}_{r,\rm bulk}(\mathbf{r})\zeta_\nu(\mathbf{r}-\mathbf{R}_J). \tag{C3}$$

Since only basis states in the immediate neighbor cells have support within the center cell, changes in the effective potential $V_c^{\rm eff}(\mathbf{r})$ only affect matrix elements in a few cells. Thus, the Hamiltonian matrix elements between basis states in the ith and jth cells will be the same as in the equivalent bulk system so long as neither basis function has support within the central cell, leading to the form of the Hamiltonian shown in Eq. (6).

Once the Hamiltonian is calculated in matrix form, an output charge density matrix $\hat{\rho}^{\rm out}$ is calculated using Eq. (10), leading to a new density in real space $\rho(\mathbf{r})$ and effective potential within the central cell $V_c^{\rm eff}[\rho(\mathbf{r})]$. This process is repeated until a predefined numerical tolerance is reached. This allows for a completely self-consistent solution to the KS equations for open systems.

APPENDIX D: BOUND STATES OF AN OPEN SYSTEM

In this appendix, we describe how one might calculate the bound states in an open system such as that of Fig. 1 and argue that this is a difficult process because bound states are solutions to a highly nonlinear eigenvalue problem. The discrete set of bound states $\{\Psi^{c^n}\}$ which is localized inside the device scattering region, can be expressed as an expansion

$$\Psi^{c^n}=\begin{cases}\varphi_l^{k_l^m}a^{k_l^m c^n}, & z\in l,\\ \psi_c^{c^n}, & z\in c,\\ \varphi_r^{k_r^m}b^{k_r^m c^n}, & z\in r,\end{cases} \tag{D1}$$

where the repeated indices k_l^m and k_r^m represent sums over only the evanescent modes. The evanescent modes $\{\varphi\}$ are obtained by diagonalizing Eq. (5) by choosing E and selecting those λ which are complex (corresponding to evanescent modes).[40]

Applying the Hamiltonian operator, we find the following homogeneous equation for Ψ^{c^n}:

$$\begin{bmatrix} A_l^{k_l^m} & h_{l,c}^E & 0\\ A_c^{k_l^m} & h_{c,c}^E & A_c^{k_r^m}\\ 0 & h_{r,c}^E & A_r^{k_r^m}\end{bmatrix}\begin{bmatrix} a^{k_l^m c^n}\\ \psi_c^{c^n}\\ b^{k_l^m c^n}\end{bmatrix}=\begin{bmatrix}0\\0\\0\end{bmatrix}. \tag{D2}$$

Here

$$A_l^{k_l^m}\equiv[h_{l,l}^E+h_{l,l-1}^E(\lambda_\varphi^{k_l^m})^{-1}]\varphi_l^{k_l^m},$$

$$A_r^{k_r^m}\equiv[h_{r,r}^E+h_{r,r+1}^E(\lambda_\varphi^{k_r^m})^{+1}]\varphi_l^{k_r^m},$$

$$A_c^{k_l^m}\equiv h_{c,l}^E\varphi_l^{k_l^m},$$

$$A_c^{k_r^m}\equiv h_{c,r}^E\varphi_r^{k_r^m}. \tag{D3}$$

The above quantities depend on the Bloch states and therefore are highly nonlinear functions of energy E.

Hence, Eq. (D2) is a highly nonlinear root finding problem for each bound state eigenvalue E, whose solution becomes a very time-consuming task. Furthermore, one does not know how many bound state there are *a priori*. We therefore conclude that it is numerically difficult to calculate them.

[1] See, for example, Chem. Eng. News May 47 (2000).

[2] M. F. Crommie, C. P. Lutz, and D. M. Eigler, Science **262**, 218 (1993).

[3] H. C. Manoharan, C. P. Lutz, and D. M. Eigler, Nature (London) **413**, 513 (2000).

[4] S. Iijima, Nature (London) **354**, 56 (1991).

[5] C. P. Collier, E. W. Wong, M. Belohradsk, F. M. Raymo, J. F. Stoddart, P. J. Kuekes, R. S. Williams, and J. R. Heath, Science **285**, 391 (1999); **289**, 1172 (2000).

[6] M. A. Reed, C. Zhou, and C. J. Muller, Science **278**, 252 (1997); J. Chen, M. A. Reed, and A. M. Rawlett, *ibid.* **286**, 1550 (1999); J. Chen, W. Wang, M. A. Reed, A. M. Rawlett, D. W. Price, and J. M. Tour, Appl. Phys. Lett. **77**, 1224 (2000).

[7] C. Joachim, J. K. Gimzewski, R. R. Shlitter, and C. Chavy, Phys. Rev. Lett. **74**, 2102 (1995); J. K. Gimzewski and C. Joachim, Science **283**, 1683 (1999).

[8] T. Rueckes, K. Kim, E. Joselevich, G. Y. Tseng, C.-L. Cheung, and C. M. Lieber, Science **289**, 94 (2000).

[9] S. J. Tans, M. H. Devoret, R. M. Alwin, and H. Dai, Nature (London) **386**, 474 (1997); S. J. Tans, J. Verschueren, R. M. Alwin, and C. Dekker, *ibid.* **393**, 49 (1998).

[10] J. W. G. Wildoeer, L. C. Venema, and A. G. Rinzler, Nature (London) **391**, 59 (1998).

[11] Y. Xue, S. Datta, S. Hong, R. Reifenberger, J. I. Henderson, and C. P. Kubiak, Phys. Rev. B **59**, 7852 (1999).

[12] A. Yazdani, D. M. Eigler, and N. Lang, Science **272**, 1921 (1996).

[13] P. L. Pernas, A. Martin-Rodero, and F. Flores, Phys. Rev. B **41**,

R8553 (1990).
[14] W. Tian and S. Datta, Phys. Rev. B **49**, 5097 (1994).
[15] L. Chico, M. P. L. Sancho, and M. C. Munoz, Phys. Rev. Lett. **81**, 1278 (1998).
[16] A. L. V. de Parga, O. S. Hernán, R. Miranda, A. L. Yeyati, N. Mingo, A. M. Martin-Rodero, and F. Flores, Phys. Rev. Lett. **80**, 357 (1998).
[17] S. N. Yaliraki, M. Kemp, and M. A. Ratner, J. Am. Chem. Soc. **121**, 3428 (1999).
[18] Y. Xue and S. Datta, Phys. Rev. Lett. **83**, 4844 (1999).
[19] E. G. Emberly and G. Kirczenow, Phys. Rev. B **60**, 6028 (1999).
[20] M. Brandbyge, N. Kobayashi, and M. Tsukada, Phys. Rev. B **60**, 17 064 (1999).
[21] H. Mehrez, J. Taylor, H. Guo, J. Wang, and C. Roland, Phys. Rev. Lett. **84**, 2682 (2000); C. Roland, M. B. Nardelli, J. Wang, and H. Guo, *ibid.* **84**, 2921 (2000).
[22] C. C. Wan, J.-L. Mozos, G. Taraschi, J. Wang, and H. Guo, Appl. Phys. Lett. **71**, 419 (1997); C. C. Wan, J. L. Mozos, J. Wang, and H. Guo, Phys. Rev. B **55**, 13 393 (1997).
[23] J. Wang, H. Guo, J.-L. Mozos, C. C. Wan, G. Taraschi, and Q. Zheng, Phys. Rev. Lett. **80**, 4277 (1998).
[24] G. Taraschi, J.-L. Mozos, C. C. Wan, H. Guo, and J. Wang, Phys. Rev. B **58**, 13 138 (1998).
[25] J. L. Mozos, C. C. Wan, G. Taraschi, J. Wang, and H. Guo, Phys. Rev. B **56**, R4351 (1997); J.-L. Mozos, C. C. Wan, G. Taraschi, J. Wang, and H. Guo, J. Phys.: Condens. Matter **10**, 2663 (1998).
[26] J. Taylor, H. Guo, and J. Wang, in *Proceedings of the Fifth International Symposium on Quantum Confinement: Nanostructures, 194th Meeting of the Electrochemical Society*, edited by M. Cahay, D. J. Lockwood, J. P. Leburton, and S. Bandyopadhyay (The Electrochemical Society, Boston, 1988), p. 640.
[27] H. J. Choi and J. Ihm, Phys. Rev. B **59**, 2267 (1999).
[28] H. J. Choi, J. Ihm, Y. G. Yoon, and S. G. Louie, Phys. Rev. B **60**, 14 009 (1999).
[29] H. J. Choi, J. Ihm, S. G. Louie, and M. L. Cohen, Phys. Rev. Lett. **84**, 2917 (2000).
[30] N. D. Lang, Phys. Rev. B **52**, 5335 (1995).
[31] K. Hirose and M. Tsukada, Phys. Rev. B **51**, 5278 (1995).
[32] N. D. Lang, Phys. Rev. B **55**, 4113 (1997).
[33] N. D. Lang and Ph. Avouris, Phys. Rev. Lett. **81**, 3515 (1998).
[34] M. Di Ventra, S. T. Pantelides, and N. D. Lang, Phys. Rev. Lett. **84**, 979 (2000).
[35] N. D. Lang and Ph. Avouris, Phys. Rev. Lett. **84**, 358 (2000).
[36] P. Hohenberg and W. Kohn, Phys. Rev. **136**, 864 (1964).
[37] W. Kohn and L. J. Sham, Phys. Rev. **140**, 1133 (1965).
[38] R. G. Parr and W. Yang, *Density-Functional Theory of Atoms and Molecules* (Oxford University Press, New York, 1989).
[39] A short account on the the *I-V* curves of a C_{60} molecular device can be found elsewhere, J. Taylor, H. Guo, and J. Wang, Phys. Rev. B **63**, 121104 (2001).
[40] Other details, including different electrode boundary conditions, formulation for multiprobes, and calculation of scattering states, etc., will be presented elsewhere. J. Taylor and Hong Guo (unpublished).
[41] For a review, see, for example, M. C. Payne, M. P. Teter, D. C. Allan, T. A. Arias, and J. D. Joannopoulos, Rev. Mod. Phys. **64**, 1045 (1992).
[42] P. Ordejón, E. Artacho, and José M. Soler, Phys. Rev. B **53**, R10 441 (1996).
[43] A. P. Jauho, N. S. Wingreen, and Y. Meir, Phys. Rev. B **50**, 5528 (1994).
[44] S. Datta, *Electronic Transport in Mesoscopic Systems* (Cambridge University Press, New York, 1995).
[45] B. G. Wang, J. Wang, and Hong Guo, Phys. Rev. Lett. **82**, 398 (1999); J. Appl. Phys. **86**, 5094 (1999).
[46] M. Brandbyge, M. R. Sorenson, and K. W. Jacobsen, Phys. Rev. B **56**, 14 956 (1997).
[47] J. C. Cuevas, A. L. Yeyati, and A. Martin-Rodero, Phys. Rev. Lett. **80**, 1066 (1998).
[48] S. Frank, P. Poncharail, Z. L. Wang, and W. A. de Heer, Science **280**, 1744 (1998).
[49] D. R. Hamann, M. Schlüter, and C. Chiang, Phys. Rev. Lett. **43**, 1494 (1982).
[50] O. F. Sankey and D. J. Niklewski, Phys. Rev. B **40**, 3979 (1989).
[51] Gianni Taraschi, M.Sc. thesis, McGill University, 1997.
[52] E. L. Briggs, D. J. Sullivan, and J. Bernholc, Phys. Rev. B **54**, 14 362 (1996).
[53] For a review, see for example, T. A. Arias, Rev. Mod. Phys. **71**, 267 (1999).
[54] D. Sánchez-Portal, P. Ordejón, E. Artacho, and J. M. Soler, Int. J. Quantum Chem. **65**, 453 (1997); E. Artacho, D. Sánchez-Portal, P. Ordejón, A. García, and J. M. Soler, Phys. Status Solidi **215**, 809 (1999); P. Ordejón, *ibid.* **217**, 335 (2000).
[55] J. Wang, Y. J. Wang, and H. Guo, J. Appl. Phys. **75**, 2721 (1994); Y. J. Wang, J. Wang, H. Guo, and E. Zaremba, Phys. Rev. B **52**, 2738 (1995).
[56] A. Brandt, Math. Comput. **31**, 333 (1977).
[57] When the open device problem is reduced to that defined over the finite central cell, energy contributions from cells outside the central must be neglected. So long as the basic variable $\rho(\mathbf{r})$ reduces to the equivalent bulk value outside the central cell, the energy contributions per unit cell outside the central will be the same as in the bulk system. Therefore, changes in the total energy can be properly evaluated and the electronic ground state determined by minimizing the energy due to states of the system in the central cell.
[58] A. R. Williams, P. J. Feibelman, and N. D. Lang, Phys. Rev. B **26**, 5433 (1982).
[59] B. Larade, J. Taylor, and H. Guo (unpublished).
[60] M. Büttiker, J. Phys.: Condens. Matter **5**, 9361 (1993).
[61] T. Christen and M. Büttiker, Europhys. Lett. **35**, 523 (1996).
[62] M. Büttiker and T. Christen, in *Quantum Transport in Semiconductor Submicron Structures*, edited by B. Kramer (Kluwer Academic, Dordrecht, 1996).
[63] Z. S. Ma, J. Wang, and H. Guo, Phys. Rev. B **57**, 9108 (1998); **59**, 7575 (1999).
[64] B. G. Wang, X. A. Zhao, J. Wang, and H. Guo, Appl. Phys. Lett. **74**, 2887 (1999); X. A. Zhao, J. Wang, and H. Guo, Phys. Rev. B **60**, 16 730 (1999).
[65] Z. Yao, H. Postma, L. Balents, and C. Deeker, Nature (London) **402**, 273 (1999); A. Bezryadin, A. R. M. Verschueren, S. J. Tans, and C. Dekker, Phys. Rev. Lett. **80**, 4036 (1998).
[66] In this work, we do not intend to review the vast literature of carbon nanotubes and refer interested readers to the following reviews: M. S. Dresselhaus, G. Dresselhaus, and P. C. Eklund, *Science of Fullerenes and Carbon Nanotubes* (Academic, San

Diego 1996); R. Saito, G. Dresselhaus, and M. S. Dresselhaus, *Physical Properties of Carbon Nanotubes*, ICP Press (World Scientific, Singapore 1998); J. Bernholc, C. Roland, and B. I. Yakobson, Crit. Rev. Solid State Mater. Sci. **2**, 706 (1997).

[67] X. Blase, L. X. Benedict, E. L. Shirley, and S. G. Louie, Phys. Rev. Lett. **72**, 1878 (1994); Y. A. Krotov, D.-H. Lee, and S. G. Louie, *ibid.* **78**, 4245 (1997); L. Chico, V. H. Crespi, L. X. Benedict, S. G. Louie, and M. L. Cohen, *ibid.*, **76**, 971 (1996); V. H. Crespi, M. L. Cohen, and A. Rubio, *ibid.* **79**, 2093 (1998); H. J. Choi, J. Ihm, S. G. Louie, and M. L. Cohen, *ibid.* **84**, 2917 (2000).

[68] R. Tamura and M. Tsukada, Phys. Rev. B **55**, 4991 (1997); **58**, 4882 (1998).

[69] M. P. Anantram and T. R. Govindan, Phys. Rev. B **58**, 4882 (1998).

[70] M. Buongiorno Nardelli, Phys. Rev. B **60**, 7228 (1999).

[71] A. Rochefort, Ph. Avouris, F. Lesage, and D. R. Salahub, Phys. Rev. B **60**, 13 824 (1999).

[72] J. W. Mintmire, B. I. Dunlap, and C. T. White, Phys. Rev. Lett. **68**, 631 (1992).

[73] N. Hamada, S. I. Sawada, and A. Oshiyama, Phys. Rev. Lett. **68**, 1579 (1992).

[74] D. S. Fisher and P. A. Lee, Phys. Rev. B **23**, 6851 (1981).

[75] M. P. López Sancho, J. M. López Sancho, and J. Rubio, J. Phys. F: Met. Phys. **14**, 1205 (1984).

[76] C. S. Jayanthi, S. Y. Wu, and J. Cocks, Phys. Rev. Lett. **69**, 1955 (1992); C. S. Jayanthi, J. Cocks, N. S. Luo, Z. L. Xie, M. Menon, and G. Yang, Phys. Rev. B **57**, 3799 (1998).

[77] S. Sanvito, C. J. Lambert, J. H. Jefferson, and A. M. Bratkovsky, Phys. Rev. B **59**, 11 936 (1999).

[78] Jeremy Taylor, Ph.D. thesis, McGill University, 2000.